SEMIANALYTICAL DESIGN OF LIBRATION POINT FORMATIONS

Sergey Trofimov, Maksim Shirobokov, Michael Koptev

Keldysh Institute of Applied Mathematics, Moscow, Russia

ABSTRACT

A novel semianalytical technique is proposed for the libration point formation design. It is based on the use of Lindstedt-Poincaré series that approximate the center manifold in the vicinity of the libration point. Any performance factor can be constructed by symbolically manipulating the series. For a number of typical formation-keeping objectives, the optimal design parameters are first obtained analytically in a low-order approximation and then exploited as an initial guess in the numerical optimization procedure for the 15th-order approximation model. The proposed technique is robust, constructive, and versatile: while avoiding the necessity of numerical integration in the highly unstable dynamical environment, we effectively use the full hierarchy of center manifold approximations. The numerical optimization for the high-order approximation model is still low-dimensional and alleviated by a good initial guess obtained from low-order approximation models.

Index Terms— Formation flying, libration point, Nelder-Mead algorithm, Lissajous orbit, Lindstedt-Poincaré series

1. INTRODUCTION

Recent advances in a whole range of small satellite technologies open the road to extensive deep space exploration. Among the promising destinations of near-future missions are the L_1 and L_2 libration points of the Sun-Earth and Earth-Moon systems. The low cost of micro- and nanospacecraft, along with their limited mass, volume, and energy capabilities, makes it natural to distribute the scientific payload across several spacecraft flying in a formation. Furthermore, it is the space-distributed measurements that are required in such applications as space weather forecasting, magnetospheric studies, space interferometry, empirical validation of fundamental physical theories, etc.

In contrast to the case of near-Earth formations, the design of a libration point formation is a much more difficult and less studied procedure. The primary obstacle is the unstable and highly nonlinear dynamics in the vicinity of the collinear libration points. The first works dated back at the beginning of the 2000s aimed at designing a continuous or impulsive control law that ensures keeping the predefined formation geometry [1–7]. The idea of concurrent numerical optimization of both formation configuration and control parameters has also been suggested [8]. At the same time, the general trend of maximally exploiting the natural dynamics was then observed, starting with the study of Howell and Marchand [9] who introduced the concept of the natural formation, a formation that keeps favorable geometry under no control (i.e., in purely ballistic motion). The efforts to explicitly describe and visualize the set of best (slowest-degrading) initial configurations for a two-spacecraft formation resulted in the notions of zero relative radial acceleration (ZRRA) [10] and zero relative acceleration and velocity (ZRAV) regions [11, 12]. All the criteria based on the relative acceleration are, however, indirect and approximate: the two spacecraft are assumed to move in close orbits with synchronized velocities. Moreover, the above notions become useless for the design of non-rigid formations with relative distances changing in a prescribed way. Even the problem of rigid formation design with three or more spacecraft is tractable only numerically. For example, in the recent works of Ferrari and Lavagna [13, 14], the genetic algorithm is utilized for global optimization.

In the current research, a novel semianalytical technique is proposed for the libration point formation design. Its foundation is the use of Lindstedt-Poincaré (LP) series that approximate the center manifold in the vicinity of the libration point. The relative motion can be described explicitly by subtracting two LP series. In the resulting series, there are just four design parameters, and non-gradient optimization methods, such as the Nelder-Mead simplex algorithm, sucessfully solve the optimal design problem. Furthermore, we can gain some insight from low-order LP approximations. Corresponding analytical estimates can be used as an initial guess in the iterative numerical optimization procedure. For complex performance metrics, these estimates appear to be crucial for the procedure to converge.

The paper is organized as follows. In Section 2, some basic information is provided about the dynamics in the vicinity of collinear libration points and the LP approximation of the relevant center manifold. Then, we introduce several performance metrics that are usually used for libration point formations. Section 4 contains the brief description of the Nelder-Mead optimization method. Analytical estimates from the linear approximation derived in Section 5, are exploited as an initial guess in the numerical optimization procedure of Section 6. The results are then adapted to the ephemeris model.

2. CENTRAL MANIFOLD DYNAMICS IN THE VICINITY OF COLLINEAR LIBRATION POINTS

2.1. Circular Restricted Three-Body Problem

In the circular restricted three-body problem (CR3BP), two celestial bodies move in circular orbits around their barycenter. The position of a spacecraft of negligible mass is usually described in the rotating barycentric reference frame, with the X-axis connecting the bodies and the Z-axis being directed along the orbital angular momentum. The equations of spacecraft motion have the following nondimensional form

$$\begin{aligned} \ddot{X} - 2\dot{Y} &= U_X \\ \ddot{Y} + 2\dot{X} &= U_Y \\ \ddot{Z} &= U_Z \end{aligned} \tag{1}$$

where

$$U(X,Y,Z) = \frac{X^2+Y^2}{2} + \frac{1-\mu}{R_1} + \frac{\mu}{R_2}$$

is the effective potential, U_X, U_Y and U_Z are the partial derivatives of U with respect to the position variables, and $\mu = m_2/(m_1+m_2)$ is the mass parameter of the system. The distances to the celestial bodies are given by the equalities

$$\begin{aligned} R_1 &= \sqrt{(X+\mu)^2+Y^2+Z^2} \\ R_2 &= \sqrt{(X-1+\mu)^2+Y^2+Z^2} \end{aligned}$$

The system (1) has five equilibrium points called libration or Lagrangian points. Three of them lying on the X-axis, are named collinear. Usually denoted by L_1, L_2, and L_3, these points are proved to be unstable. In the Sun-Earth system, the coordinates of the L_1 and L_2 points are as follows:

$$X_{L1} = 0.9899871, \quad X_{L2} = 1.0100740$$

It is the latter point that we will focus on in this study.

2.2. Linearization About the Collinear Libration Point

Before linearizing the equations of motion about the L_1 or L_2 libration point, it is convenient to make a change of variables

$$x = \frac{X - X_L}{D}, \quad y = \frac{Y}{D}, \quad z = \frac{Z}{D}$$

where X_L is the X-coordinate of the libration point (L_1 or L_2), and $D = |X_L - 1 + \mu|$ is the distance from this libration point to the smaller celestial body. Then, the evolution of the position and velocity vectors $\mathbf{r} = (x,y,z)^T$, $\dot{\mathbf{r}} = (\dot{x},\dot{y},\dot{z})^T$ is described in the linear approximation by the differential equations

$$\begin{bmatrix} \dot{\mathbf{r}} \\ \ddot{\mathbf{r}} \end{bmatrix} = \begin{bmatrix} \mathbf{O}_{3\times3} & \mathbf{I}_{3\times3} \\ \mathbf{U} & -2\boldsymbol{\Omega} \end{bmatrix} \begin{bmatrix} \mathbf{r} \\ \dot{\mathbf{r}} \end{bmatrix} \tag{2}$$

Here $\mathbf{O}_{3\times3}$ and $\mathbf{I}_{3\times3}$ are respectively the zero matrix and the indentity matrix of 3×3 size,

$$\boldsymbol{\Omega} = \begin{bmatrix} 0 & -1 & 0 \\ 1 & 0 & 0 \\ 0 & 0 & 0 \end{bmatrix}$$

and $\mathbf{U}$ is the matrix of second-order partial derivatives of the effective potential estimated in the libration point:

$$\mathbf{U} = \begin{bmatrix} 1+2\bar{\mu} & 0 & 0 \\ 0 & 1-\bar{\mu} & 0 \\ 0 & 0 & -\bar{\mu} \end{bmatrix}$$

where

$$\bar{\mu} = \frac{\mu}{|X_L - 1 + \mu|^3} + \frac{1-\mu}{|X_L + \mu|^3}$$

The matrix of the system (2) has a pair of real eigenvalues and two pairs of imaginary eigenvalues. They have a form of $\pm i\omega_p$ and $\pm i\omega_v$. The phase space is thus of a saddle $\times$ center $\times$ center type. Quasi-periodic Lissajous orbits from the four-dimensional central manifold can be represented as

$$\begin{aligned} x &= \alpha \cos(\omega_p t + \phi_1) \\ y &= -\kappa\alpha \sin(\omega_p t + \phi_1) \\ z &= \beta \cos(\omega_v t + \phi_2) \end{aligned} \tag{3}$$

The constants α and β play a role of the in-plane and out-of-plane amplitudes; ϕ_1 and ϕ_2 are the arbitrary phases, and

$$\kappa = \frac{\omega_p^2 + 2\omega_v^2 + 1}{2\omega_p}$$

In the Sun-Earth system, the planar and vertical frequencies ω_p and ω_v are respectively equal to 2.0864519 and 2.0152089 for the L_1 point; for the L_2 point, their values are 2.0570158 and 1.9850765.

2.3. Lindstedt-Poincaré Series

The LP series expansion explicitly parameterizes—up to the user-specified degree of accuracy—the invariant tori the center manifold is foliated by. In particular, the manifolds consisting of periodic and quasi-periodic libration point orbits can be approximated by the LP series.

The general expressions of order n for the Lissajous orbits have the following complex exponential form [15]:

$$\begin{aligned} x &= \sum x_{ijkm}\, \alpha^i \beta^j \gamma_1^k \gamma_2^m \\ y &= \sqrt{-1} \sum y_{ijkm}\, \alpha^i \beta^j \gamma_1^k \gamma_2^m \\ z &= \sum z_{ijkm}\, \alpha^i \beta^j \gamma_1^k \gamma_2^m \end{aligned} \tag{4}$$

Here $\gamma_i = \exp\left[\sqrt{-1}\,(\omega_i t + \phi_i)\right]$, and the summation is performed over the indices satisfying the conditions $I = \{\, i, j \geq 0,\ |k| \leq i,\ |m| \leq j,\ 1 \leq i + j \leq n\}$. The frequencies ω_1 and ω_2 are also expanded:

$$\begin{aligned} \omega_1 &= \omega_p + \sum d_{ij}\, \alpha^i \beta^j \\ \omega_2 &= \omega_v + \sum f_{ij}\, \alpha^i \beta^j \end{aligned} \tag{5}$$

The indices in Eq. (5) are summed over the positive even numbers. The LP series for halo orbits, three-dimensional periodic orbits branching from the family of planar orbits, can be found in [16]. The expressions resemble Eq. (4), except for the fact that a single frequency $\omega = \omega_1 = \omega_2$ appears and the additional condition for such a resonance is required to be satisfied. We further concentrate on the family of Lissajous orbits, though the methodology proposed can also be applied to halo orbit formations and corresponding LP series.

The larger the Lissajous orbit, the more distant it is from the libration point. As a result, the LP series of higher order are required to approximate the center manifold with the same precision. In Fig. 1 adapted from the famous monograph [17], the limit values of in-plane and out-of-plane amplitudes are shown for which the LP series of 5th, 15th, and 35th order give an error not larger than 10^{-6} non-dimensional units (one unit for the Sun-Earth system is about 1.5 mln km) at the interval of π time units.

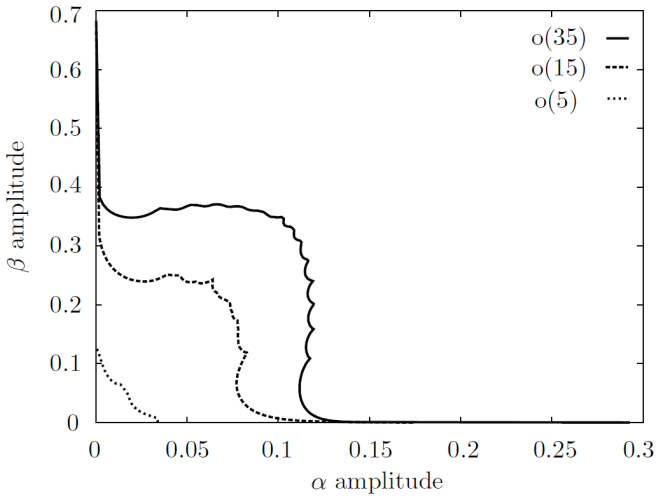

Fig. 1: LP series approximation order required for Lissajous orbits of different in-plane and out-of-plane amplitudes [17]

3. REFERENCE ORBIT AND FORMATION PERFORMANCE METRICS

In this research, the Lissajous orbit around the Sun-Earth L_2 point with $\alpha = 110,000$ km and $\beta = 90,000$ km is used as the reference orbit. Such dimensions are close to those of the orbit of the Gaia space telescope succesfully launched in 2013 [18]. The three-dimensional view and the yz-projection of the reference orbit in the linear approximation are demonstrated in Fig. 2. As Fig. 1 reveals, the 15th order of series is enough to approximate the reference orbit accurately. The corrected 3D-view and the yz-projection are given by Fig. 3.

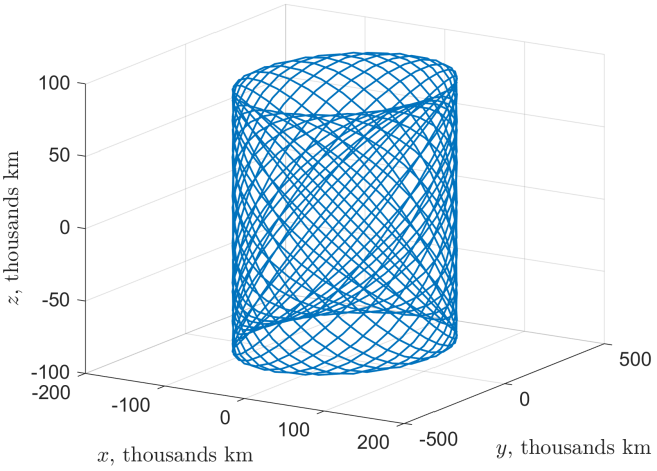

(a) 3D view

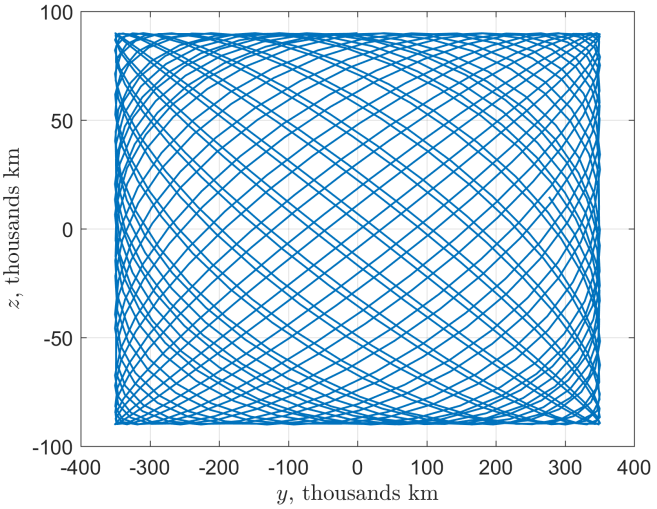

(b) yz-projection

Fig. 2: Reference orbit in the linear approximation

The values of the planar frequency ω_1 obtained from the 15th-order LP approximation of Lissajous orbits with the in-plane and out-of-plane amplitudes up to 150,000 km are depicted in Fig. 4. The same plot for the vertical frequency ω_2 is represented by Fig. 5. Though the relative change of each frequency is rather small, their difference can decrease up to one third (see Fig. 6). For example, for the reference orbit, the difference between $\omega_1 = 2.0490816$ and $\omega_2 = 1.9865984$ is 0.0624832, 13% less than $\omega_p - \omega_v = 0.0719393$. This fact will be further used to improve some analytical estimates.

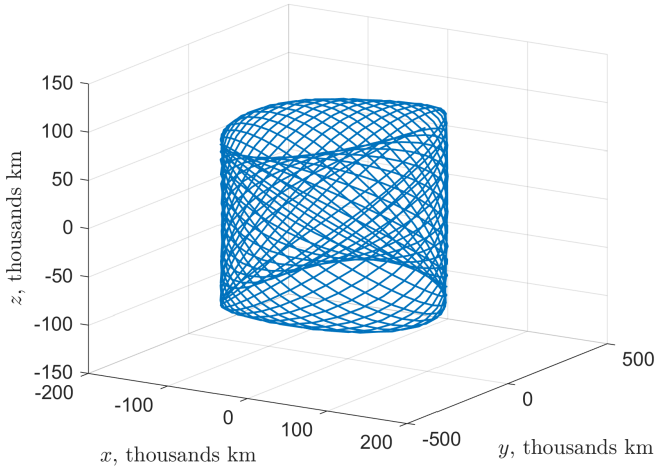

(a) 3D view

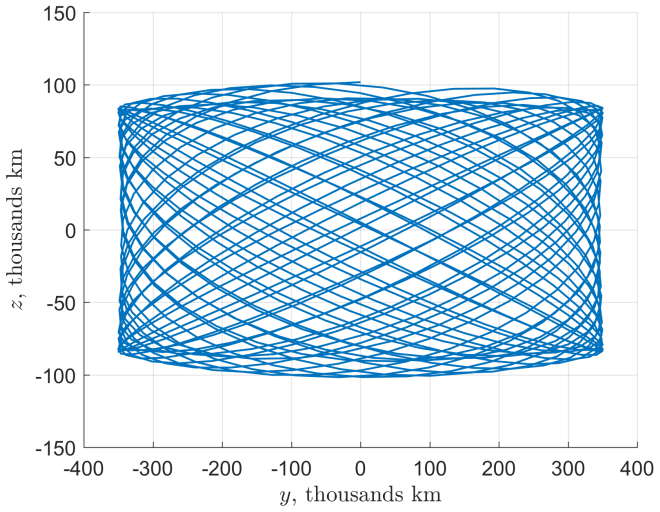

(b) yz-projection

Fig. 3: Reference orbit in the 15th-order LP approximation

The reference orbit approximated by the LP series expansion of any order is described by four parameters: two amplitudes α, β and two phases ϕ_1, ϕ_2. Assuming the first spacecraft in a two-spacecraft formation moves along the reference orbit, the relative position vector

$$\Delta\mathbf{r} = \mathbf{r}_2 - \mathbf{r}_1 = \begin{bmatrix} x_2 - x_1 \\ y_2 - y_1 \\ z_2 - z_1 \end{bmatrix} \equiv \begin{bmatrix} \Delta x \\ \Delta y \\ \Delta z \end{bmatrix}$$

can be readily expanded in LP series by subtracting the series for the components of $\mathbf{r}_2$ and $\mathbf{r}_1$. The resulting LP expansions for Δx, Δy, and Δz can be parameterized by two differential amplitudes $\Delta\alpha$, $\Delta\beta$ and two differential phases $\Delta\phi_1$, $\Delta\phi_2$.

To measure the performance of a formation, some scalar performance metric is usually introduced. If the relative distance is of primary interest in the mission, it is convenient to target the required interval of values for the squared distance

$$\Delta r^2 = \Delta x^2 + \Delta y^2 + \Delta z^2$$

The relevant LP series can be derived symbolically or, in case of the linear approximation, even by hand (see Section 5).

When a projection of the relative trajectory onto the plane with the unit normal vector $\mathbf{n} = (n_x, n_y, n_z)^T$ is tracked, the following metric can be used:

$$\Delta r^2 - (\Delta\mathbf{r}\cdot\mathbf{n})^2 = \left(1 - n_x^2\right)\Delta x^2 + \left(1 - n_y^2\right)\Delta y^2 + \\ + \left(1 - n_z^2\right)\Delta z^2 - 2n_x n_y \Delta x \Delta y - 2n_y n_z \Delta y \Delta z - \\ - 2n_x n_z \Delta x \Delta z$$

If the projection plane is fixed in the rotating reference frame, $\mathbf{n}$ is a constant vector. For an inertially fixed plane, the normal vector is a function of time:

$$\mathbf{n} = \begin{bmatrix} n_{x0}\cos t + n_{y0}\sin t \\ n_{y0}\cos t - n_{x0}\sin t \\ n_z \end{bmatrix}$$

This situation is typical for space interferometry missions.

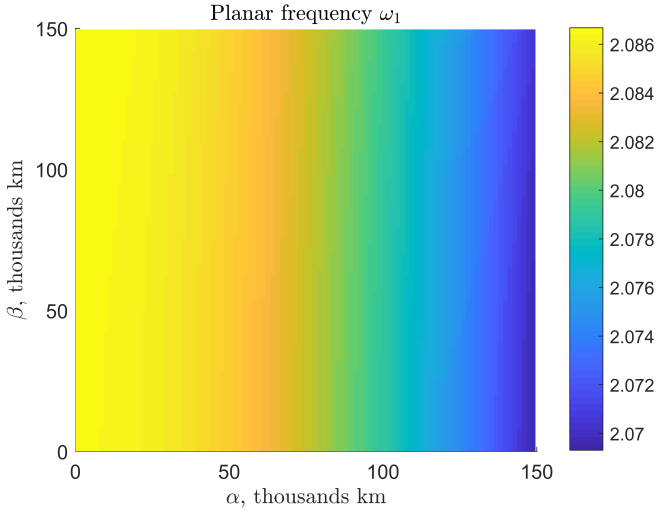

Fig. 4: Planar frequency of Lissajous orbits as a function of the in-plane and out-of-plane amplitudes

A more complex metric is required if two spacecraft are to be aligned along a given direction specified by the unit vector $\mathbf{n}$. The straightforward candidate is the squared cosine of the angle between the relative position vector $\Delta\mathbf{r}$ and $\mathbf{n}$:

$$\cos^2\gamma = \frac{(\Delta\mathbf{r}\cdot\mathbf{n})^2}{\Delta r^2}$$

For formations of three and more spacecraft, performance metrics can be constructed in a similar fashion based on pairwise relative distances. With adding one more spacecraft, the

number of design variables increases by 4. What is important, it does not depend on the order of LP series approximation.

Another critical advantage of the proposed approach is the ability to compute the performance metric without the necessity of numerical integration in the highly unstable dynamical environment. It is also better to avoid the derivative computations due to the highly irregular search space. Along with the relatively small number of optimized variables, this all speaks in favor of derivative-free numerical optimization techniques.

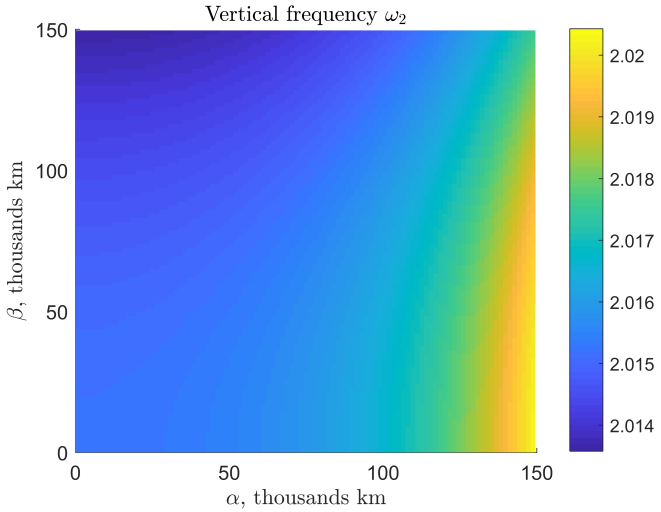

Fig. 5: Vertical frequency of Lissajous orbits as a function of the in-plane and out-of-plane amplitudes

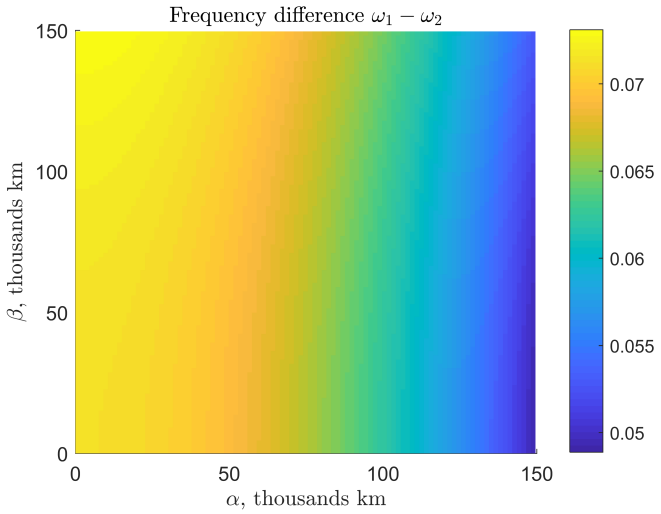

Fig. 6: Difference between the planar and vertical frequencies for Lissajous orbits with different amplitudes

4. NELDER-MEAD OPTIMIZATION ALGORITHM

One of the popular non-gradient methods for solving unconstrained optimization problems is the Nelder-Mead simplex method (do not confuse with the simplex method for linear programming problems). The idea behind the method is first to initialize a simplex with $n+1$ vertices in the n-dimensional phase space and then to modify the simplex with the operations of reflection, expansion, contraction, and shrinkage, depending on the objective function values at the vertices. The algorithm is simple and easily programmable. Its description can be found in the paper of Lagarias et al. [19]. This classical algorithm is implemented in the FMINSEARCH routine, a part of the Matlab Optimization Toolbox.

In cases when the problem is initially constrained, penalty functions are added to the objective function. For example, if we want to target some value c of the relative distance so that $c\,(1-\varepsilon_1) \le \Delta r \le c\,(1+\varepsilon_2)$ at a specific time interval, the following objective function can be exploited:

$$J = \left(\langle \Delta r \rangle - c\right)^2 + k_1 \max\left(0, c\,(1-\varepsilon_1) - m\right) + \\ + k_2 \max\left(0, M - c\,(1+\varepsilon_2)\right) \tag{6}$$

In this expression, $\langle \Delta r \rangle$ is the average value of $\sqrt{\Delta r^2}$ over a given time interval, $m = \min \sqrt{\Delta r^2}$, $M = \max \sqrt{\Delta r^2}$, k_1 and k_2 are some large penalty weight coefficients.

In practice, the Nelder-Mead method often performs well even for irregular, non-smooth, and noised objective functions or objective functions with dense local minima in a vicinity of one global minimum. However, when the dimension of the phase space is high, convergence to a local minimum could take much time; so, it is usually recommended to use the classical Nelder-Mead algorithm only for small-scale problems. Nonetheless, large-scale modifications of the algorithm also exist [20, 21]. These parallel versions can be effectively used in high-performance computing systems.

5. ANALYTICAL ESTIMATES BASED ON THE LINEAR APPROXIMATION

It is of vital importance to properly initialize almost any optimization algorithm. The role of an initial guess grows with the increase of computational complexity of the problem (for instance, when the number of optimized variables is large). It appears that a good initial guess and performance metric estimates in the problem of libration point formation design can be obtained from the linear approximation.

In a two-spacecraft formation, the relative position vector $\Delta\mathbf{r}$ satisfies the same linearized equations of motion (2) as do the position vectors of both spacecraft. Thus, the solution can be written in the same form as Eq. (3):

$$\Delta x = A_x \cos\left(\omega_p t + \theta_1\right)$$

$$\Delta y = -\kappa A_x \sin\left(\omega_p t + \theta_1\right)$$

$$\Delta z = A_z \cos\left(\omega_v t + \theta_2\right)$$

The transformation formulas between the relative amplitudes and phases A_x, A_z, θ_1, θ_2 and the above mentioned differential parameters $\Delta\alpha$, $\Delta\beta$, $\Delta\phi_1$, $\Delta\phi_2$ are derived in Appendix.

In the linear approximation, the squared relative distance is expressed as

$$\Delta r^2 = \frac{A_x^2\left(\kappa^2+1\right)+A_z^2}{2} + \frac{A_z^2}{2}\cos\left(2\omega_v t + 2\theta_2\right) - \\ - \frac{A_x^2\left(\kappa^2-1\right)}{2}\cos\left(2\omega_p t + 2\theta_1\right)$$

It exhibits beating around the mean value

$$c^2 = \frac{A_x^2\left(\kappa^2+1\right)+A_z^2}{2}$$

with the beat frequency $\delta = \omega_p - \omega_v$ (see Fig. 7).

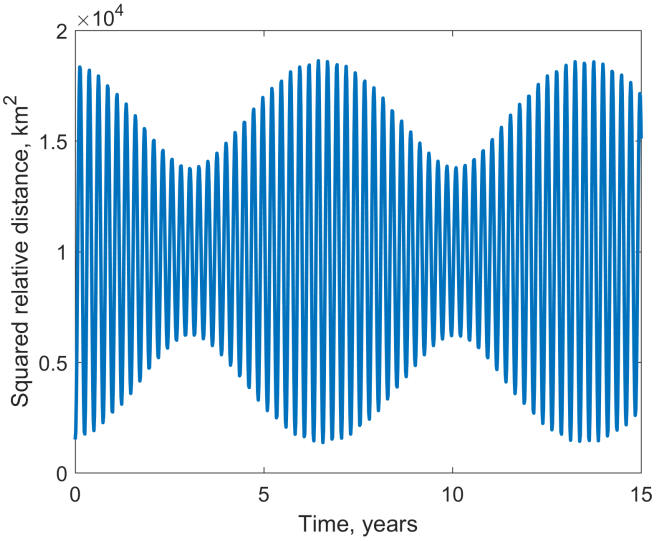

Fig. 7: Squared relative distance beating behavior

It follows from the beating theory that the upper and lower envelopes for the sum of two harmonics

$$a\cos\left(\omega t+\varphi\right) + b\cos\left(\left(\omega+\Delta\omega\right)t+\varphi+\Delta\varphi\right)$$

are determined by the functions

$$\pm\sqrt{a^2+b^2+2ab\cos\left(\Delta\omega\cdot t+\Delta\varphi\right)}$$

with the plus sign corresponding to the upper envelope. In our notation,

$$a = \frac{A_z^2}{2},\quad b = -\frac{A_x^2\left(\kappa^2-1\right)}{2},\quad \Delta\omega = 2\delta,\quad \Delta\varphi = -2\Delta\theta$$

where $\Delta\theta = \theta_2 - \theta_1$. So, the upper envelope has a form of

$$\sqrt{\frac{A_x^4\left(\kappa^2-1\right)^2}{4}+\frac{A_z^4}{4}-\frac{A_x^2A_z^2\left(\kappa^2-1\right)}{2}\cos\left(2\delta t-2\Delta\theta\right)}$$

For long time intervals, the extrema of the upper and lower envelopes representing the maximum and minimum values of Δr^2 significantly deviate from the mean value c^2. Indeed, the relative deviation

$$\frac{\max\left|\Delta r^2 - c^2\right|}{c^2} = \frac{A_z^2 + A_x^2\left(\kappa^2-1\right)}{A_z^2 + A_x^2\left(\kappa^2+1\right)}$$

has a minimum of

$$\chi = \frac{\kappa^2-1}{\kappa^2+1} \approx 0.82$$

when $A_z = 0$. The distance between the spacecraft oscillates from $\sqrt{0.18\,c^2} \approx 0.42\,c$ to $\sqrt{1.82\,c^2} \approx 1.35\,c$ in this case. Such variations would almost always be unacceptable in a real mission. However, it is important for us to observe that, if the harmonics interfere destructively, a time interval exists during which the squared relative distance values are confined within a strip of arbitrarily small width 2ε centered at c^2. The larger the width, the longer this interval. To maximize its length for a given ε, we need to select the amplitudes A_x and A_z so that the distance between the adjacent roots of the equation

$$\sqrt{\frac{A_x^4\left(\kappa^2-1\right)^2}{4}+\frac{A_z^4}{4}-\frac{A_x^2A_z^2\left(\kappa^2-1\right)}{2}\cos\left(2\delta t-2\Delta\theta\right)} = c^2\varepsilon$$

with respect to t is maximum. Returning to the short notation in terms of a and b, this equation can be rearranged as

$$\cos\left(2\delta t-2\Delta\theta\right) = \frac{c^4\varepsilon^2-a^2-b^2}{2ab}$$

Taking into account the mean value constraint

$$a - b/\chi = c^2$$

yields

$$\cos\left(2\delta t-2\Delta\theta\right) = \frac{c^4\varepsilon^2-a^2-\chi^2\left(a-c^2\right)^2}{2\chi a\left(a-c^2\right)}$$

The maximum distance between the roots is attained when the right-hand side is minimum. Dividing both the numerator and the denominator by c^4 and introducing the notation

$$\xi = 1-\frac{a}{c^2},\quad \xi\in[0,1]$$

we obtain the equivalent function to be minimized:

$$\eta\left(\xi\right) = \frac{\left(1-\xi\right)^2+\chi^2\xi^2-\varepsilon^2}{2\chi\xi\left(1-\xi\right)}$$

The graphs of its natural logarithm for some ε values are plotted in Fig. 8 near the minimum point. This point

$$\xi_{\min} = \frac{1-\varepsilon^2-\sqrt{\left(1-\varepsilon^2\right)\left(\chi^2-\varepsilon^2\right)}}{1-\chi^2}$$

does not depend on ε and can therefore be estimated with the assumption $\varepsilon = 0$:

$$\xi_{\min} \approx \frac{1}{1+\chi} \approx 0.55$$

It results in the relationship

$$a = -b = \frac{\kappa^2 - 1}{2\kappa^2}\, c^2$$

or, in terms of the amplitudes,

$$A_x = \frac{c}{\kappa}, \quad A_z = \frac{c}{\kappa}\sqrt{\kappa^2 - 1} \tag{7}$$

The upper envelope curve is now determined by the function

$$\frac{c^2}{\kappa^2}\left(\kappa^2 - 1\right)\left|\sin\left(\delta t - \Delta\theta\right)\right|$$

To start with a favorable destructive interference interval (see Fig. 9), it is required to tune the relative phase difference $\Delta\theta$. Up to an integer multiple of π,

$$|\Delta\theta| = \arcsin\left(\frac{\varepsilon\kappa^2}{\kappa^2 - 1}\right) \tag{8}$$

Then, the squared distance remains close enough (i.e., within the 2ε-strip) to the mean value over the interval $[0, T]$ where

$$T = \frac{2\,|\Delta\theta|}{\delta} \tag{9}$$

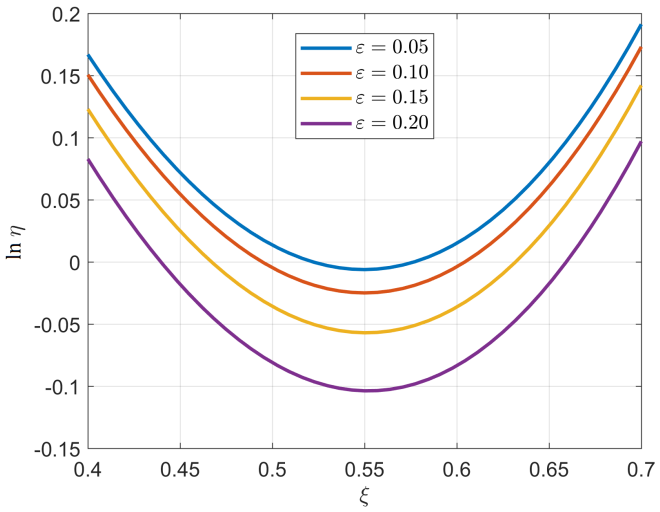

Fig. 8: $\ln\eta$ as a function of ξ in the $[0.4, 0.7]$ interval

The formulas (7-9) can be exploited as an initial guess in a numerical optimization procedure in case we aim at designing a two-spacecraft formation with the target relative distance c. The Nelder-Mead method can then be applied to the objective function (6) with $\varepsilon_1 = 1 - \sqrt{1-\varepsilon}$, $\varepsilon_2 = \sqrt{1+\varepsilon} - 1$. One of the phases, θ_1 or θ_2, can be initialized arbitrarily. For small ε values, the relative distance is symmetrically constrained near the mean value c by the bounds $c\,(1 - \varepsilon/2)$ and $c\,(1 + \varepsilon/2)$.

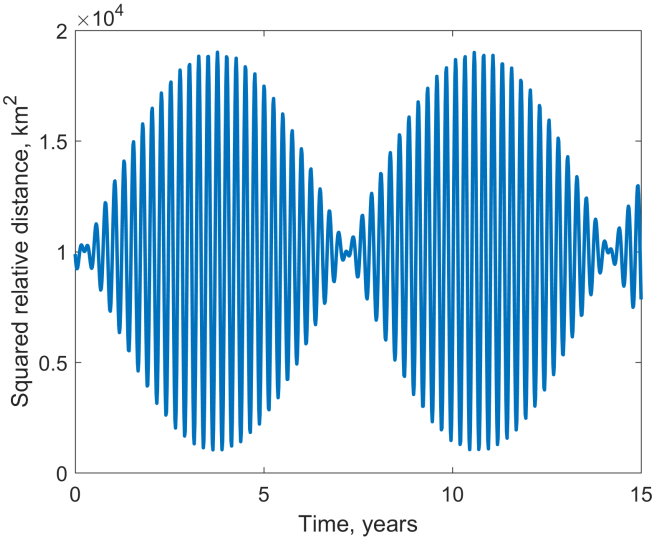

(a) 15-year interval

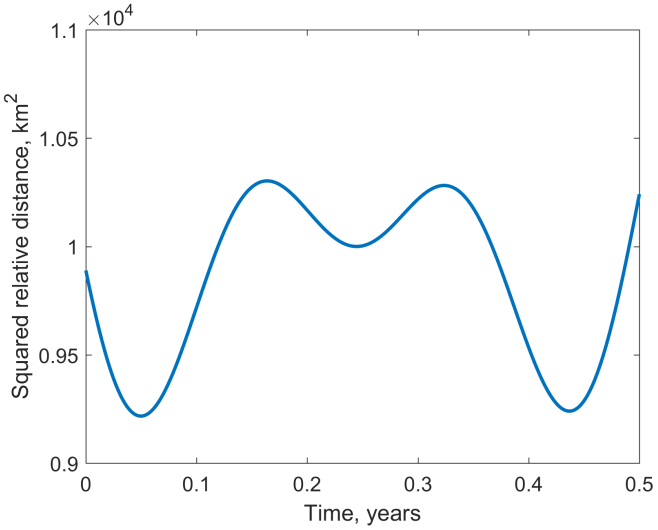

(b) First half-year interval enlarged

Fig. 9: Behavior of the squared relative distance analytically optimized for $c = 100$ km, $\varepsilon = 0.1$

In case of other formation performance metrics, analytical estimates can also often be derived in a similar fashion.

It turns out to be surprisingly simple to analytically obtain an initial guess in the case of a three-spacecraft formation that is supposed to move as an equilateral triangle. After repeating the above analysis for all the three pairs of spacecraft, we can straightforwardly deduce that both the relative amplitudes A_x, A_z and the phase difference $|\Delta\theta|$ (up to an integer multiple of 2π) should be equal in these pairs. Indeed, they obey the same

relationships (7)-(8), with c being the desired side length of an equilateral triangle. This leads to the expressions

$$x_2 - x_1 = A_x \cos(\omega_p t + \theta_1)$$

$$y_2 - y_1 = -\kappa A_x \sin(\omega_p t + \theta_1)$$

$$z_2 - z_1 = A_z \cos(\omega_v t + \theta_2)$$

and

$$x_3 - x_2 = A_x \cos(\omega_p t + \theta_3)$$

$$y_3 - y_2 = -\kappa A_x \sin(\omega_p t + \theta_3)$$

$$z_3 - z_2 = A_z \cos(\omega_v t + \theta_4)$$

as well as

$$x_3 - x_1 = A_x \cos(\omega_p t + \theta_5)$$

$$y_3 - y_1 = -\kappa A_x \sin(\omega_p t + \theta_5)$$

$$z_3 - z_1 = A_z \cos(\omega_v t + \theta_6)$$

where $|\theta_2 - \theta_1| = |\theta_4 - \theta_3| = |\theta_6 - \theta_5| \equiv |\Delta\theta| \pmod{\pi}$. At the same time, since $x_3 - x_1 = (x_3 - x_2) + (x_2 - x_1)$ and $z_3 - z_1 = (z_3 - z_2) + (z_2 - z_1)$, the equalities

$$|\theta_3 - \theta_1| = \frac{2\pi}{3} \pmod{2\pi}$$

$$|\theta_4 - \theta_2| = \frac{2\pi}{3} \pmod{2\pi}$$

should hold. For example, one can take

$$\theta_3 = \theta_1 + \frac{2\pi}{3}$$

$$\theta_4 = \theta_2 + \frac{2\pi}{3}$$

Then

$$\theta_5 = \theta_1 + \frac{\pi}{3}$$

$$\theta_6 = \theta_2 + \frac{\pi}{3}$$

Along with the equalities

$$\theta_2 - \theta_1 = \theta_4 - \theta_3 = \theta_6 - \theta_5 = \arcsin\left(\frac{\varepsilon\kappa^2}{\kappa^2 - 1}\right)$$

and Eq. (7), these relations allow us to complete the design of an equilateral triangle formation.

6. NUMERICAL OPTIMIZATION AND ADAPTATION TO THE EPHEMERIS MODEL

The derived analytical estimates can be exploited as an initial guess for the Nelder-Mead optimization procedure in a high-order LP approximation model. As justified in Section 3, the 15th order of the LP series expansion is quite accurate for the reference Lissajous orbit selected. The termination tolerances of Matlab's FMINSEARCH routine for the objective function and the vector of optimized variables have been set to $1\mathrm{e}-8$.

In the relative distance-based performance metric (6) with $c = 6.6845871 \cdot 10^{-7}$ (the non-dimensional equivalent of 100 km), the penalty weight coefficients k_1 and k_2 both equal 10^7. The analytical estimate (9) for the time a formation naturally keeps acceptable performance is used as the length of the optimization interval.

The numerical optimization in the 15th-order approximation model is followed by the adaptation of resulting absolute spacecraft trajectories to the high-fidelity model incorporating the gravitational attraction of the Sun and all the planets up to Saturn, as well as the solar radiation pressure force (the area-to-mass-ratio of 0.01 m^2/kg is assumed for all spacecraft). In all the examples below, the initial date of Jan 1, 2020 is used. It requires just 3-8 multiple-shooting iterations to converge.

The evolution of the relative distance for a two-spacecraft formation in several models of motion is compactly shown in Fig. 10. The upper and lower bounds $\varepsilon_1 = 1 - \sqrt{1-\varepsilon}$, $\varepsilon_2 = \sqrt{1+\varepsilon} - 1$ with $\varepsilon = 0.1$ are indicated by dashed lines. In the 15th-order approximation model, the analytical guess slightly violates the bounds, which is then successfully eliminated by the numerical optimization. The subsequent adaptation to the ephemeris model has almost no influence on the performance.

For a three-spacecraft formation designed to move in the equilateral triangle configuration, each relative distance curve in Fig. 10 is replaced by the triplet of pairwise distance curves. These four triplets are depicted separately in Figs. 11-14. The optimized initial configuration ensures that during half a year of natural motion all the pairwise relative distances are within the $\pm 5\%$ band centered at the desired value of 100 km. Other observations are also similar to those for a two-spacecraft formation.

It is worth underlining that the presence of an analytically derived initial guess is often crucial. For instance, in the case of a two-spacecraft formation, the number of iterations for the Nelder-Mead method to converge more than quadruples if the trivial initial guess of zero differential amplitudes is used (i.e., spacecraft orbits are initially considered identical). Moreover, for a three-spacecraft formation, such a guess does not lead to convergence at all.

In higher orders of approximation, the difference between the planar and vertical frequencies is known to be less than in the linear approximation. Thus, the conservative estimate (9) can usually be refined by substituting $\omega_2 - \omega_1$ in the denominator instead of $\delta = \omega_p - \omega_v$. The analytical guess sometimes appears excellent even for longer intervals. For example, it is managed to optimize the half-year formation design of Fig. 10 over the one-year interval (Fig. 15). In some cases, however, it is necessary to relax the ε tolerance when proceeding to the numerical optimization. For sophisticated performance metrics, natural constraints on ε can exist in high-fidelity models.

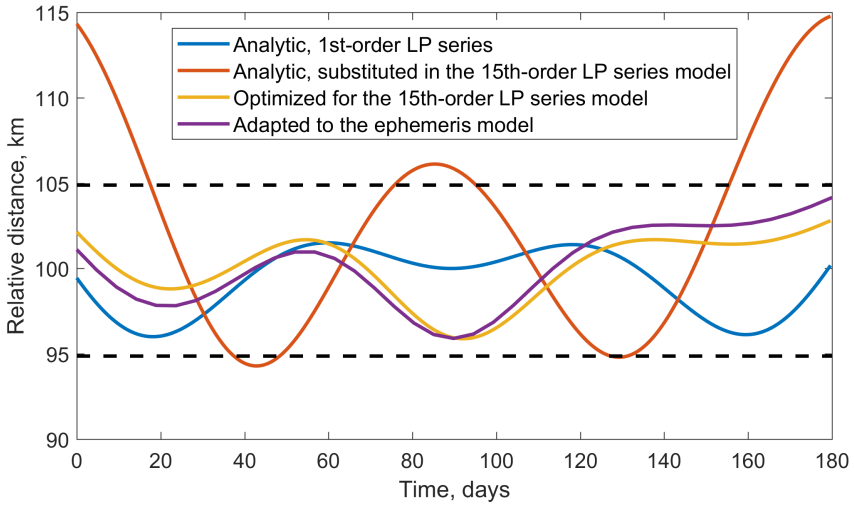

Fig. 10: Relative distance behavior for a two-spacecraft formation in different models of motion

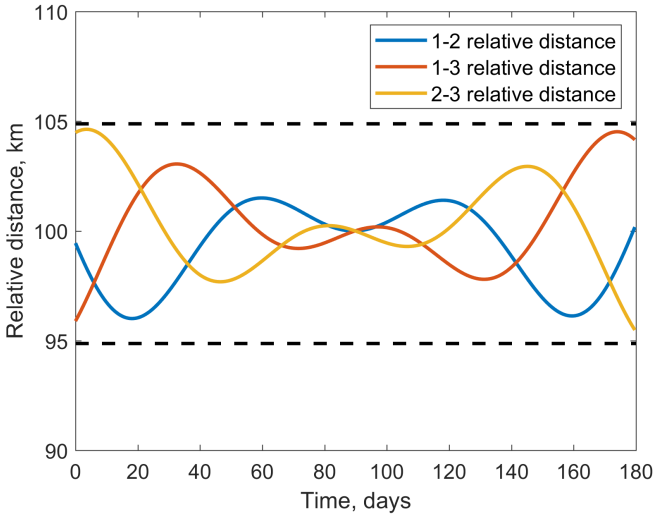

Fig. 11: Optimal solution to the problem of linearized relative motion in an almost equilateral formation

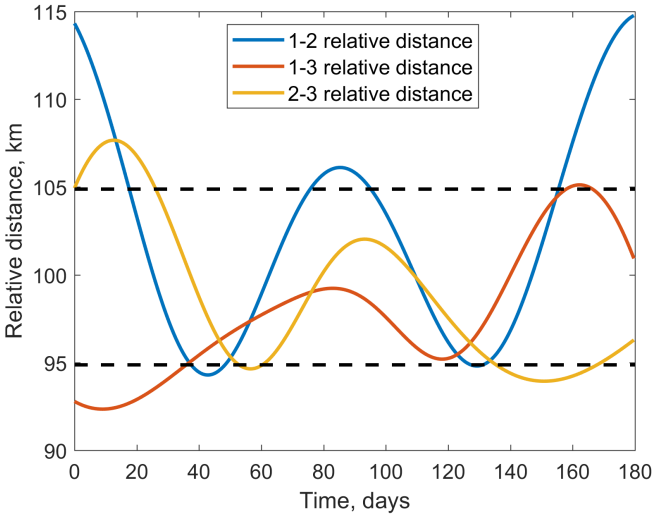

Fig. 12: Optimal solution to the problem of linearized relative motion in an almost equilateral triangle formation substituted to the 15th-order LP approximation model

7. CONCLUSIONS

The proposed semianalytical technique based on the powerful tool of Lindstedt-Poincaré series has appeared to be an effective approach to the rather complicated problem of designing libration point formations with various performance metrics. The series of any order are readily parameterized by just four design parameters, which opens the road to such non-gradient optimization techniques as the classical Nelder-Mead simplex algorithm. Numerical integration is thus totally avoided.

The analysis of low-order expressions for the performance metric makes it often possible to obtain an initial guess for the numerical optimization procedure. This drastically speeds up the convergence or is even its prerequisite.

The explicit analytical derivations have been presented for the relative distance-based performance metric in the cases of two-spacecraft and three-spacecraft formations. The optimal design is found so that the relative distance variations for half a year are no greater than 5-6% in the 15th-order approximation model and the ephemeris model. The same stability level proved to be achievable for the one-year ballistic flight.

8. ACKNOWLEDGMENTS

The research is supported by the Russian Science Foundation grant 17-71-10242.

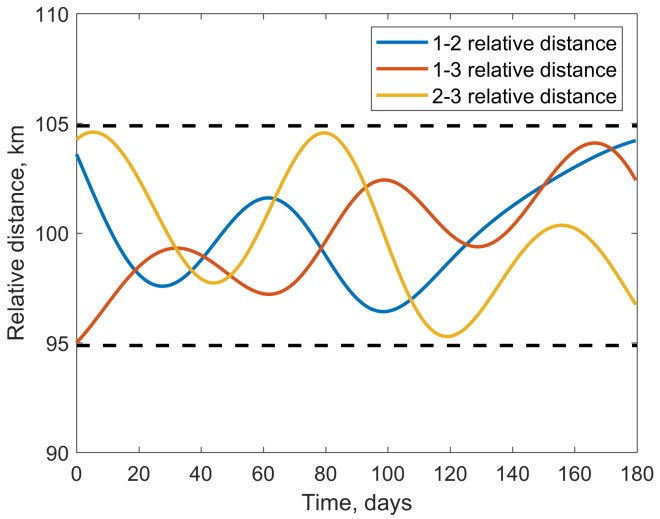

Fig. 13: Numerically optimized relative motion in an almost equilateral triangle formation based on the initial guess from the linearized model of motion

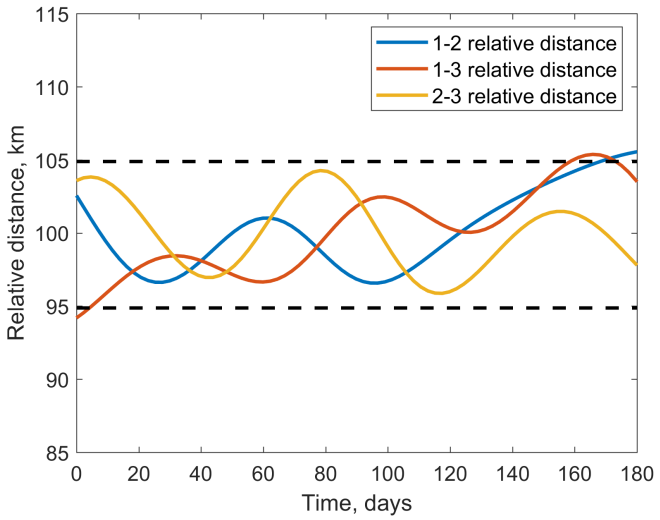

Fig. 14: Adaptation of the solution numerically optimized in the 15th-order approximation model to the ephemeris model

9. REFERENCES

[1] P. Gurfil and N.J. Casdin, "Dynamics and Control of Spacecraft Formation Flying in Three-Body Trajectories," in *AIAA Guidance, Navigation, and Control Conference and Exhibit*, Montreal, Canada, August 6-9, 2001, 11 p.

[2] N.H. Hamilton, D. Folta, and R. Carpenter, "Formation Flying Satellite Control Around the L2 Sun-Earth Libration Point," in *AIAA/AAS Astrodynamics Specialist Conference and Exhibit*, Monterey, CA, USA, August 5-8, 2002, 11 p.

[3] D.J. Scheeres, F.Y. Hsiao, and N.X. Vinh, "Stabilizing Motion Relative to an Unstable Orbit: Applications to Spacecraft Formation Flight," *Journal of Guidance, Control, and Dynamics*, vol. 26, no. 1, pp. 62–73, 2003.

[4] F.Y. Hsiao and D.J. Scheeres, "Design of Spacecraft Formation Orbits Relative to a Stabilized Trajectory," *Journal of Guidance, Control, and Dynamics*, vol. 28, no. 4, pp. 782–794, 2005.

[5] B.G. Marchand and K.C. Howell, "Control Strategies for Formation Flight in the Vicinity of the Libration Points," *Journal of Guidance, Control, and Dynamics*, vol. 28, no. 6, pp. 1210–1219, 2005.

[6] B.G. Marchand and S.A. Stanton, "Actuator Constrained Optimal Formation Keeping Near the Libration Points," *Journal of the Astronautical Sciences*, vol. 57, no. 3, pp. 607–632, 2009.

[7] E. Serpelloni, M. Maggiore, and C.J. Damaren, "Control of Spacecraft Formations Around the Libration Points Using Electric Motors with One Bit of Resolution," *Journal of the Astronautical Sciences*, vol. 61, no. 4, pp. 367–390, 2014.

[8] S.I. Infeld, S.B. Josselyn, W. Murray, and I.M. Ross, "Design and Control of Libration Point Spacecraft Formations," *Journal of Guidance, Control, and Dynamics*, vol. 30, no. 4, pp. 899–909, 2007.

[9] B.G. Marchand and K.C. Howell, "Natural and Non-Natural Spacecraft Formations Near the L1 and L2 Libration Points in the Sun-Earth/Moon Ephemeris System," *Dynamical Systems: an International Journal, Special Issue on Mechanics and Space Mission Design*, vol. 20, no. 1, pp. 149–173, 2005.

[10] G. Gómez, M. Marcote, J. Masdemont, and J. Mondelo, "Zero Relative Radial Acceleration Cones and Controlled Motions Suitable for Formation Flying," *Journal of the Astronautical Sciences*, vol. 53, no. 4, pp. 413–431, 2005.

[11] A. Héritier and K.C. Howell, "Regions Near the Libration Points Suitable to Maintain Multiple Spacecraft," in *AIAA/AAS Astrodynamics Specialist Conference*, Minneapolis, MN, USA, August 13-16 2012, p. 20.

[12] A. Héritier and K.C. Howell, "Dynamical Evolution of Natural Formations in Libration Point Orbits in a Multi-Body Regime," *Acta Astronautica*, vol. 102, pp. 332–340, 2014.

[13] F. Ferrari and M. Lavagna, "Optimization of Triangular Formation Flying Configurations Under the Circular and

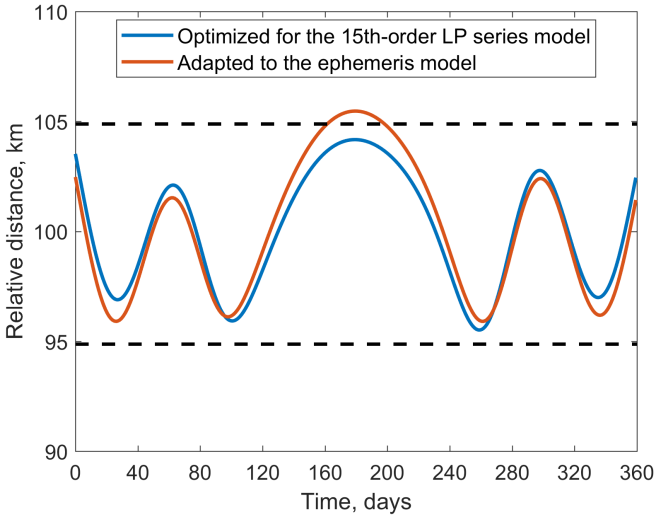

Fig. 15: Relative distance behavior for a two-spacecraft formation optimized over the extended time interval

Elliptic Three-Body Problem Dynamics Modelling," in *25th International Symposium of Space Flight Dynamics (ISSFD)*, Munich, Germany, October 19-23, 2015, 17 p.

[14] F. Ferrari and M. Lavagna, "Suitable Configurations for Triangular Formation Flying About Collinear Libration Points Under the Circular and Elliptic Restricted Three-Body Problems," *Acta Astronautica*, vol. 147, pp. 374–382, 2018.

[15] G. Gómez, À. Jorba, J. Masdemont, and C. Simó, *Dynamics and Mission Design Near Libration Point Orbits – Volume III: Advanced Methods for Collinear Points*, vol. 4, World Scientific, 2001.

[16] G. Gómez, J. Llibre, R. Martínez, and C. Simó, *Dynamics and Mission Design Near Libration Point Orbits – Volume I: Fundamentals: The Case of Collinear Libration Points*, vol. 4, World Scientific, 2001.

[17] W.S. Koon, M.W. Lo, J.E. Marsden, and S.D. Ross, *Dynamical Systems, the Three-Body Problem and Space Mission Design*, Springer-Verlag, 2008.

[18] F. Renk and M. Landgraf, "Gaia: Trajectory Design with Tightening Constraints," in *24th International Symposium of Space Flight Dynamics (ISSFD)*, Laurel, MD, USA, May 5-9, 2014, 18 p.

[19] J.C. Lagarias, J.A. Reeds, M.H. Wright, and P.E. Wright, "Convergence Properties of the Nelder-Mead Simplex Method in Low Dimensions," *SIAM Journal on Optimization*, vol. 9, no. 1, pp. 112–147, 1998.

[20] D. Lee and M. Wiswall, "A Parallel Implementation of the Simplex Function Minimization Routine," *Computational Economics*, vol. 30, no. 2, pp. 308–313, 2007.

[21] K. Klein and J. Neira, "Nelder-Mead Simplex Optimization Routine for Large-Scale Problems: A Distributed Memory Implementation," *Computational Economics*, vol. 43, no. 4, pp. 447–461, 2014.

10. APPENDIX – TRANSFORMATION BETWEEN RELATIVE AND DIFFERENTIAL PARAMETERS OF LINEARIZED RELATIVE MOTION

The orbit of the first spacecraft is described by the expressions

$$x_1 = \alpha \cos(\omega_p t + \phi_1)$$
$$y_1 = -\kappa\alpha \sin(\omega_p t + \phi_1)$$
$$z_1 = \beta \cos(\omega_v t + \phi_2),$$

For the orbit of the second spacecraft, we have

$$x_2 = (\alpha + \Delta\alpha) \cos(\omega_p t + \phi_1 + \Delta\phi_1)$$
$$y_2 = -\kappa(\alpha + \Delta\alpha) \sin(\omega_p t + \phi_1 + \Delta\phi_1)$$
$$z_2 = (\beta + \Delta\beta) \cos(\omega_v t + \phi_2 + \Delta\phi_2)$$

Since the relative position vector $\Delta\mathbf{r}$ satisfies the same linear equations, its components can be written as follows:

$$\Delta x = A_x \cos(\omega_p t + \theta_1)$$
$$\Delta y = -\kappa A_x \sin(\omega_p t + \theta_1)$$
$$\Delta z = A_z \cos(\omega_v t + \theta_2)$$

The relation between A_x, A_z, θ_1, θ_2 and $\Delta\alpha$, $\Delta\beta$, $\Delta\phi_1$, $\Delta\phi_2$ can be easily derived from the equations $\Delta x = x_2 - x_1$, $\Delta y = y_2 - y_1$, $\Delta z = z_2 - z_1$. The solution is given by the following relationships:

$$\Delta\phi_1 = \arctan(A_x \sin(\theta_1 - \phi_1), A_x \cos(\theta_1 - \phi_1) + \alpha)$$
$$\Delta\phi_2 = \arctan(A_z \sin(\theta_2 - \phi_2), A_z \cos(\theta_2 - \phi_2) + \beta)$$
$$\Delta\alpha = -\alpha + \alpha \cos\Delta\phi_1 + A_x \cos(\theta_1 - \phi_1 - \Delta\phi_1)$$
$$\Delta\beta = -\beta + \beta \cos\Delta\phi_2 + A_z \cos(\theta_2 - \phi_2 - \Delta\phi_2)$$